American Journal of Engineering and Applied Sciences

Original Research Paper

XPS Studies of the SiO_2 Substrates and Thermoelectric Thin Films of $Sn/Sn+SnO_2$ under the Effects of the Different Thermal Treatments

[1]Mebougna Drabo, [2]Satilmis Budak, [2]Stephen Egarievwe and [1]Richard Lagle

[1]Department of Mechanical and Civil Engineering, Alabama A&M University, Normal, AL USA
[2]Department of Electrical Engineering and Computer Science, Alabama A&M University, Normal, AL USA

Article history
Received: 02-09-2020
Revised: 28-12-2020
Accepted: 08-01-2021

Corresponding Author:
Satilmis Budak
Department of Electrical Engineering and Computer Science, Alabama A&M University, Normal, AL USA
Email: satilmis.budak@aamu.edu

Abstract: Multilayered thermoelectric $Sn/Sn+SnO_2$ thin films were prepared using KJL DC/RF magnetron sputtering system under Ar gas plasma on the SiO_2 substrates. The thicknesses of the fabricated thin films were found using Filmetrics UV thickness measurement system. The fabricated thin films were annealed at different temperatures for one hour to tailor the thermoelectric properties. In this study, unannealed, annealed at 150 and 300°C samples were characterized using Thermo Fisher XPS system brought to the Alabama A&M University by the NSF-MRI support. X-ray Photoelectron Spectroscopy (XPS), also known as Electron Spectroscopy for Chemical Analysis (ESCA) is a type of analysis used for characterization of various surface materials. XPS is mostly known for the characterization of thin films-which are coatings that have been deposited onto a substrate and may be comprised of many different materials to alter or enhance the substrate's performance. XPS analysis provides information for composition, chemical states, depth profile, imaging and thickness of thin film. This paper focuses on the application of XPS techniques in thin film research for $Sn/Sn+SnO_2$ multilayered thermoelectric system and SiO_2 substrates annealed at different temperatures. Since SiO_2 substrates were used during the deposition of the multilayer thin films, we would like to perform detailed XPS studies on the SiO_2 substrates. SiO_2 substrates is being used with many researchers, this manuscript will be good reference for the researchers using SiO_2 substrates. Thermal treatment of the substrates and the multilayered thin films has caused some changes of the XPS characterization including binding energy, depth profile, peak value and FWHM. The treatment effects were discussed and compared to each other.

Keywords: XPS, ECSA, Thin Film, Substrate and Deposition

Introduction

Thin film is not a novel application, with its earliest use recorded as a glaze to mitigate the porosity of pottery in 890 B.C. (Gould *et al*., 2017). It was also recognized for its potential usability in optics by Hooke, Newton and others in the 17th century. Since then, there has been more research on thin film and its uses. Different materials with varying absorption/refraction and fluorescence have been developed and used for many different applications.

There is a continuously increasing demand for high-performance materials. An essential component for the performance of a material is its surface. The surface of a material is an integral point where an external environment interacts with the material. These chemical and physical interactions are what may affect the performance of a material. Specifically, the surface may influence the corrosion rate, catalytic activity, adhesive properties and other factors (Thermo Scientific XPS, 2020). A well-known method and standard tool for surface analysis is X-ray Photoelectron Spectroscopy (XPS).

X-Ray Photoelectron Spectroscopy (XPS) Theory and Application

X-ray Photoelectron Spectroscopy (XPS) is a form of electron spectroscopy it is also known as Electron

Spectroscopy for Chemical Analysis (ESCA) (Thermo Scientific XPS, 2020) and is utilized as a type of surface analysis technique (Geng *et al*., 2002). By utilizing XPS, it is possible to analyze the surface chemistry and/or elemental composition of a material; additionally, XPS can measure the chemical and electronic state of the elements within the material (Thermo Scientific XPS, 2020). XPS requires an understanding of the photoemission process as well as the characterization of the surface of the material being analyzed shown in Fig. 1 and 2.

Due to the surface of the material representing a discontinuity, when an electron is moving through a solid, there is a probability that it will lose all or part of its energy due to an inelastic collision, the average distance travelled prior to such a collision occurring is known as the inelastic mean free path (NACK Network, Pennsylvania State University, 2018). In XPS the energy used ranges between 50-1200 eV as such the values of the inelastic mean free path are very small. This means that the photoelectrons must originate from the atomic layers at the very top of the surface in order to be detected and as such this makes XPS highly surface-specific and thus, appropriate characterization of the surface is necessary (NACK Network, Pennsylvania State University, 2018; Thermo Scientific XPS, 2020). As shown in Fig. 1, when using XPS, we categorize the characteristics of the surface by the number of atomic layers or by the thickness in nanometers.

In order to obtain XPS spectra, the chosen material is irradiated with a beam of monochromatic X-rays. This results in the emission of photoelectrons via the Photoemission Process which is based on Einstein's photoelectric effect (NACK Network, Pennsylvania State University, 2018). By absorbing incident X-rays photoelectrons are emitted as shown in Fig. 2.

Simultaneously, the Kinetic Energy of the electrons being emitted from the top 1-10 nm of the material's surface are measured. The entire XPS process is shown in Fig. 3.

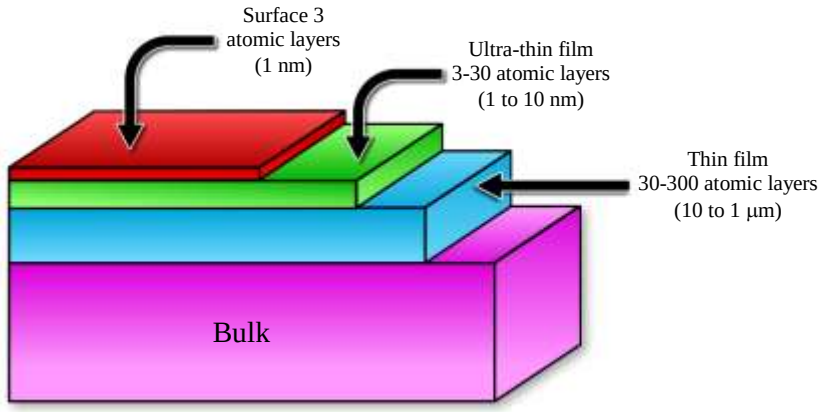

Fig. 1: Surface characterization and properties

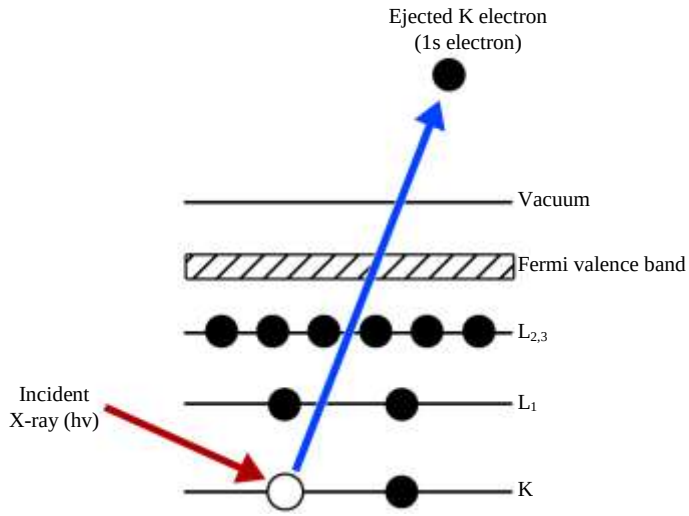

Fig. 2: The photoemission process

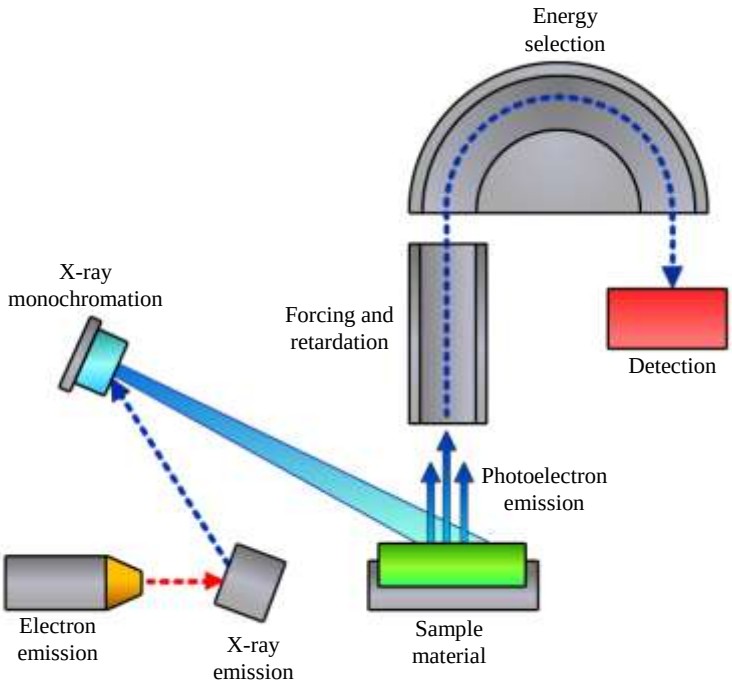

Fig. 3: XPS process

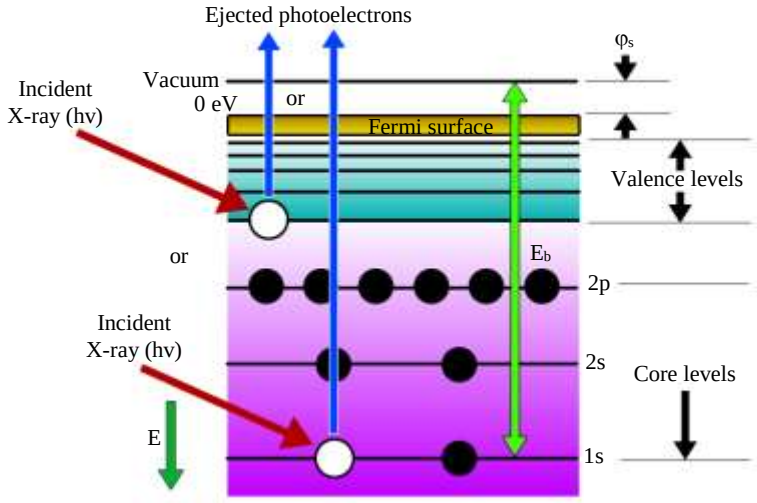

Fig. 4: Kinetic energy and binding energy relationship

By applying these principles an XPS spectra can be formed by plotting the number of ejected electrons detected (Intensity) versus their associated binding energy (NACK Network, Pennsylvania State University, 2018; Thermo Scientific XPS, 2020). The spectra can also be obtained by measuring the number of ejected electrons over a range of electron kinetic energies. This is due to the fact that the kinetic energy of the emitted electron is directly related to its binding energy as shown in Equation 1 and in Fig. 4. Peaks emerge in the spectrum from atoms emitting electrons of a specific characteristic energy. The energies of the photoelectron peaks allow the identification and quantification of all surface elements (hydrogen and helium were once thought to be exceptions to this rule, but recent research has shown that they may be measured in XPS spectra (Zhong *et al*., 2018). The spectroscopy results are typically the measurements of the elemental composition and electron activity within the surface (1-10 nm) of a material (Thermo Scientific XPS, 2020):

$$E_k = h\nu - E_b - \varphi_{sp} \quad (1)$$

$$\nu = \frac{c}{\lambda} \quad (2)$$

In Equation 1, E_k is the kinetic energy of the ejected electron, E_b is the binding energy of the electron to the atom, h is Planck's constant and ν is the frequency of the incident x-ray which is calculated by using Equation 2. where C is the speed of light and λ is the wavelength of the X-ray. Finally, φ_{sp} is the spectrometer work function, this is a correction factor that is specific to the detector. This is needed as the Fermi energies of the sample and the spectrometer coincide as the electrons from the sample are transferred to the spectrometer until said Fermi energies are aligned as shown in Fig. 4 (Washington State University and Scudiero, 2019).

XPS spectra are, for the most part, quantified in terms of peak intensities and peak positions. The peak intensities measure how much of a material is at the surface, while the peak positions indicate the elemental and chemical composition. Other values, such as the Full Width at Half Maximum (FWHM) are useful indicators of chemical state changes and physical influences. That is, broadening of a peak may indicate: A change in the number of chemical bonds contributing to a peak shape, a change in the sample condition (x-ray damage) and/or differential charging of the surface (localized differences in the charge state of the surface) (Casa XPS, 2020).

XPS spectra are, for the most part, quantified in terms of peak intensities and peak positions. The peak intensities measure how much of a material is at the surface, while the peak positions indicate the elemental and chemical composition. Other values, such as the Full Width at Half Maximum (FWHM) are useful indicators of chemical state changes and physical influences. That is, broadening of a peak may indicate: A change in the number of chemical bonds contributing to a peak shape, a change in the sample condition (x-ray damage) and/or differential charging of the surface (localized differences in the charge state of the surface) (Casa XPS, 2020).

Thin Film

Thin film is a layer or coating ranging from 0.1 nm-100 μm in thickness and can be comprised of many different materials, from metals, to oxides, to compounds (Xie *et al*., 2014). Both the thickness and material of the thin film is useful when determining its functionality. Thin films have many different applications depending on their properties and may be used in memory discs, heat sinks, solar cells, optics, LED displays and other ways, but they are most commonly associated with being used as a semiconductor (Fig. 5, Table 1). Thin films are formed via deposition onto a substrate (Fig. 6). Deposition is an additive process by which a thin film is added and its thickness is controlled. There are many different types of deposition techniques, but these may generally be categorized into two main categories-physical and chemical Table 2) (Teixeira *et al*., 2011). Substrates may also be comprised of various materials and the thin film may be leveraged to alter or enhance the substrate's performance. XPS analysis is able to give insight into the surface properties and characterization of thin films.

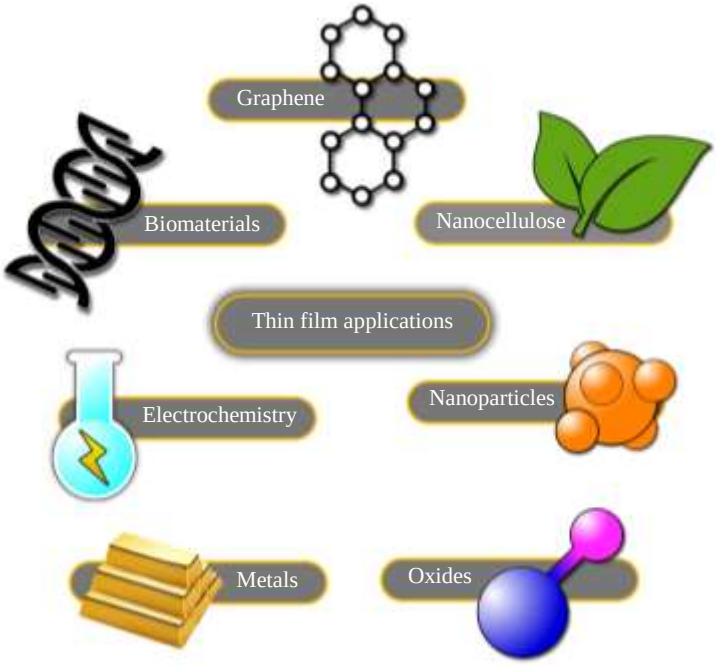

Fig. 5: Examples of thin film applications

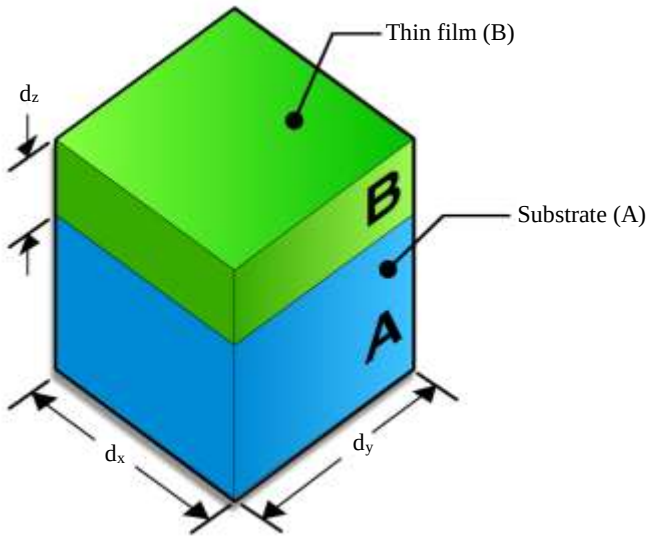

Fig. 6: Example of thin film deposition on the substrate in which A represents the substrate, B represents the thin film with dz thickness having a lateral extension dx,y >> dz

Table 1: Examples of thin film semiconductor applications (Koçak, 2018)

Application field	Examples
Optics	• Anti-reflection coating; on Tenses or solar cells • Refraction coatings for minors • Coatings to produce decorations (Color; luster) • Interference filters • CO's DVD's and upcoming Ds • Waveguides • Photosensitive coating of 'analog' film for old cameras
Chemistry	• Diffusion Barriers • Protection against corrosion/oxidation • Sensors for liquid/gaseous chemicals
Mechanics	• "Hard" layers (e.g., on drill bits) • Adhesion providers • Friction reduction
Magnetics	• "Hard" discs • Video/Audio tape • "SQUIDS"
Electricity (without semi-conductors)	• Insulating/conducting films, e.g., for resistors, capacitors • Piezoelectric devices

Table 2: Thin film deposition techniques (Koçak, 2018)

Thin film deposition techniques			
Physical		Chemical	
Sputtering	Evaporation	Gas phase	Liquid phase
Glow discharge D.C. sputtering	Vacuum evaporation	Chemical vapor deposition	Electro-deposition
Triode sputtering	Resistive heating evaporation	Layer chemical vapor deposition	Chemical Bath Deposition (CBD) Arrest Precipitation Technique (APT)
Getter sputtering	Flash evaporation	Photo-chemical vapor deposition	Electro less deposition
Radio frequency sputtering		Plasma enhanced vapor deposition	Anodization Liquid Phase Epitaxy
Magnetic sputtering Ion beam sputtering	Electron beam evaporation	Metal-Organo Chemical Vapor Deposition (MO-CVD)	Sol-Gel Spin Coating Spray-Pyrolysis Technique (SPT)
A.C. Sputtering	Arc R.F. Heating		Ultrasonic (SPT) Polymer Assisted Deposition (PAD)

XPS Analysis of Thin Film and Thickness Determination

XPS examines the elemental composition of a thin film. The spectra analysis will inform the reviewer of what elements are present in a sample, as well as the concentrations of each element and the oxidation state. In the past, thin film was determined by comparing the peak intensities of similar elemental compounds. For example, a study conducted by (Seah *et al*., 2004) was on the measurement of SiO_2 thin film based on the analysis of the Si and Si_4^+ 2p peaks of Si and SiO_2, respectively. There are still ways that XPS analysis is continuously being enhanced and improved to give more precise results in its applications.

In a study conducted by (Mao *et al*., 2008) an algorithm was formed to rectify some inaccuracies of XPS quantification on the measurement of a surface's thickness. The researchers used a W/SiO_2 over-layer sample with consideration of the background in a region of about 100 eV following the film signal peak. They tested their algorithm using the analysis strategy of Tougaard (Equation 3). After using the associated equations to establish a relationship between thickness and energy, the calculated and/or measured spectra for different known thicknesses were used to specify the intensity curve (Equation 4). According to their method, the thickness could be determined using a given calculated curve $I(E)$ from the intersection of the normalized experimental spectrum $J(E)$ and the $I(E)$ curve (using Eq. 5) (Mao *et al*., 2008):

$$F(E) = J(E) - B_1 \int_E^{E_{\max}} J(E') \frac{E' - E}{\left[C + (E' - E)^2\right]} dE' \quad (3)$$

Equation 3. The Tougaard background correction for a measured spectrum $J(E)$ where $F(E)$ is the flux of electrons excited from atoms with kinetic energy E and C is a parameter. B_1 is used as adjusting zero intensity at a certain energy, which is considered to be the lower limit of the peak area, the upper limit of the peak area being $E_{\max}$ (Mao *et al*., 2008):

$$E = E_S - \propto d \quad (4)$$

Equation 4. A linear equation representing the relationship between thickness and energy where E is the energy at which the background intensity is measured, E_s is the chosen starting energy for film thickness $d = 0$, α is a parameter which specifies a proper spectrum energy region concerned (Mao *et al*., 2008):

$$I(E) = \frac{\beta(E_S - E)}{1 - \exp\left[-\frac{E_S - E}{\alpha\lambda_i}\right] + \gamma \exp\left[-\frac{E_S - E}{\alpha\zeta}\right]} \quad (5)$$

Equation 5. The numerator represents the fact that $I(E)$ is almost linear with d before the normalization and the denominator which represents the effect due to normalization (Mao *et al*., 2008).

Materials and Methods

X-ray Photoelectron Spectroscopy (XPS) is a good technique for determining dominant surface composition of materials. XPS analysis provides information for composition, chemical states, depth profile, imaging and thickness of thin film. This paper focuses on the application of XPS on the SiO_2 substrates and the thin film research of $Sn/Sn+SnO_2$ multilayered thermoelectric systems. Thermal treatment; such as annealing, of the multilayered thin films has caused some changes to the XPS surface characterization including binding energy, depth profile, peak value and FWHM. The treatment effects were discussed and compared to each other. In this study the Thermo-Fisher XPS system was used and is shown in Fig. 7. The XPS system is equipped with analysis software that identifies the binding energies of the surface species.

The alternating layers of Sn and $Sn+SnO_2$ were prepared using Kurt J. Lesker (KJL) DC/RF magnetron sputtering. The background vacuum was about 1×10^{-5} Torr before the deposition started. During the deposition of the multilayer deposition the vacuum was about 3×10^{-3} Torr. After the background vacuum was reached, Ar gas was introduced to get plasma for DC and RF sputtering. After the first layer of Sn was deposited, the shutter for SnO_2 was also opened and the two guns for Sn and SnO_2 run at the same time.

After 1 min of each alternation layer deposition, the shutter for SnO_2 was turned on and off. After 50 multilayers of thin film was deposited, the shutters were closed and then deposition was stopped and the chamber was purged with N_2 gas to take out the fabricated multilayer thin films out. The thickness of the fabricated thermoelectric thin films was measured using Filmetrics UV thickness measurement system. The results of the measurement of the thickness were shown on the Fig. 8. The total thickness of the fabricated multilayer thermoelectric devices were measured as 574.75 nm.

Fig. 7: High-performance XPS surface analysis system by Thermo Fisher

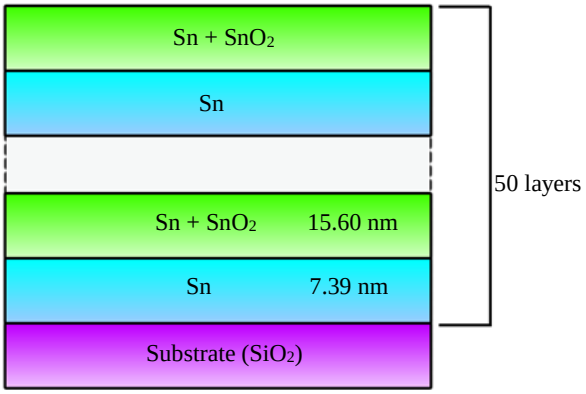

Fig. 8: Geometry for the Sn/Sn+SnO_2 thin films

The thermoelectric multilayer thin films were annealed at different temperatures to improve the efficiency of the thermoelectric devices. Some of the annealed samples were characterized using Thermo-Fisher XPS instrument at different conditions including different X-ray energies. The gathered data and analysis were given in part 3 (Results and Discussions). Results and discussion part has two parts (a) XPS studies on the SiO_2 substrates, (b) XPS studies on Sn/Sn+SnO_2 multilayered thin films.

Results and Discussion

XPS Studies on the SiO_2 Substrates

As we discussed in the previous part "XPS is a type of surface analysis technique that utilizes irradiated x-rays to analyze the energy of photoelectrons generated by the photoelectric effect (Geng *et al*., 2002)." The Fig. 9a-9c shows Sn scans for un-annealed SiO_2 substrates at different X-ray etching energies and at different etch levels from the surface of the SiO_2 substrates through deeper levels. *The term used here in this manuscript as X-ray etch means Ar ion etching at 1000, 2000 and 4000 eV etching.* During the analysis, instead of "unannealed" wording, "temperature at 0 annealing" term was used. Etch level 0 shows the surface of the thin film. As seen from Fig. 9a, counts vs Binding energies show clear distinction depending on the x-ray energy from 1000 to 4000 eV. It seems that the energy of 1000 eV yields more counts at the surface (etch level 0). The sample in Fig. 9a was scanned with respect to Binding energy of values from 483.78 to 486.78 eV. Yields (counts) in Fig. 9b and 6c increase for the x-ray energy of 4000 eV when the etch levels are chosen for 10 and 19. That might give some idea, the higher energy could affect the counts in the deeper levels. The yields for different x-ray energy levels at the etch level of 19, the scanning with respect to binding energy of the counts clear in much and clearly separated from each other. This might give us the etched level of 19 of the SiO_2 substrate produces more homogeneous distribution of the yields with respect to the binding energy.

The Fig. 10a-10c shows Sn scans for annealed SiO_2 substrate at 150°C at different X-ray etching energies and at different etch levels from the surface of SiO_2 substrate through deeper levels. During the analysis, instead of "annealed at 150°C" wording, "temperature at 150°C" term was used. Etch level 0 shows the surface of SiO_2 substrate. As seen from Fig. 10a-10c, counts Vs Binding energies show looks like approaching to each other depending on the x-ray energy from 1000 to 4000 eV. The sample in Fig. 10a-10c was scanned with respect to Binding energy of values from 482.78 to 487.78 eV. Yields (counts) in Fig. 10b and 10c increase for the x-ray energies from 1000 to 4000 eV when the etch levels are chosen for 10 and 19. That might give some idea, the higher energy could affect the counts in the deeper levels. The binding energy levels are little bit different than the cases for the unannealed cases.

Figure 11a-11c shows Sn scans for annealed thin film at 300°C at different X-ray etching energies and at different etch levels from the SiO_2 substrates through deeper levels. During the analysis, instead of "annealed at 300°" wording, "temperature at 300°C" term was used. Etch level 0 shows the surface of the thin film. As seen from Fig. 11a, counts vs Binding energies show looks like approaching to each other depending on the x-ray energy for 2000 and 4000 eV even if the yield is much higher for the case of x-ray etching power at 1000 eV. The sample in Fig. 11a-11c was scanned with respect to Binding energy of values from 483.78 to 486.78 eV. Yields (counts) in Fig. 11b and 11c decrease for the x-ray energies from 1000 to 4000 eV when the etch levels are chosen for 10 and 19 with respect to the etch level of 0. That might give some idea, the higher energy could affect the counts in the deeper levels in negative direction unlike the cases in un-annealed and annealed at 150°C cases.

Figure 12a-12c show average counts at different annealing temperatures. The wording of "annealing temperature of 0 C" was used for "un-annealed case", the wording of "annealing temperature of 150°C" was used for "annealed SiO_2 substrates at 150°C", the wording of "annealing temperature of 300°C" was used for "annealed thin film at 300°C". Average counts vs etch line # were plotted for three different cases of x-ray energies of 1000, 2000 and 4000 eV in Fig. 12a-12c. As seen from Fig. 12a, average count values increase when the x-ray energy increased while the etch line # increased. Etch # means the data were collected from the deeper level with respect to the surface of SiO_2 substrates. The average counts vs etch-# data were collected when the SiO_2 substrates was not annealed in Fig. 12a.

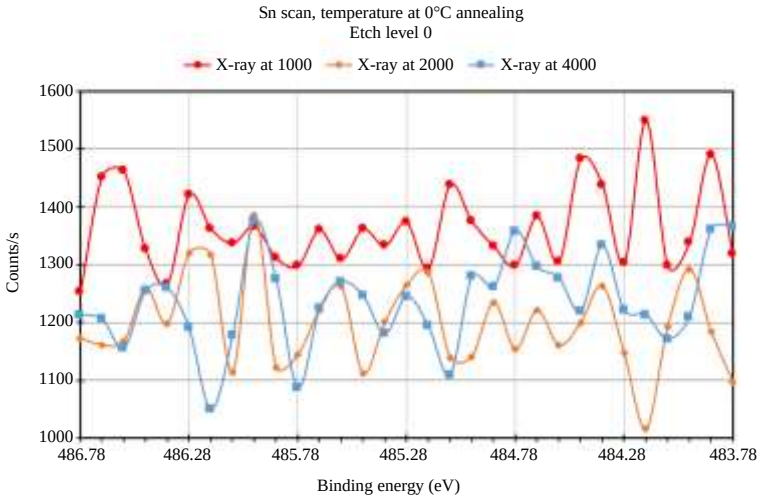

(a)

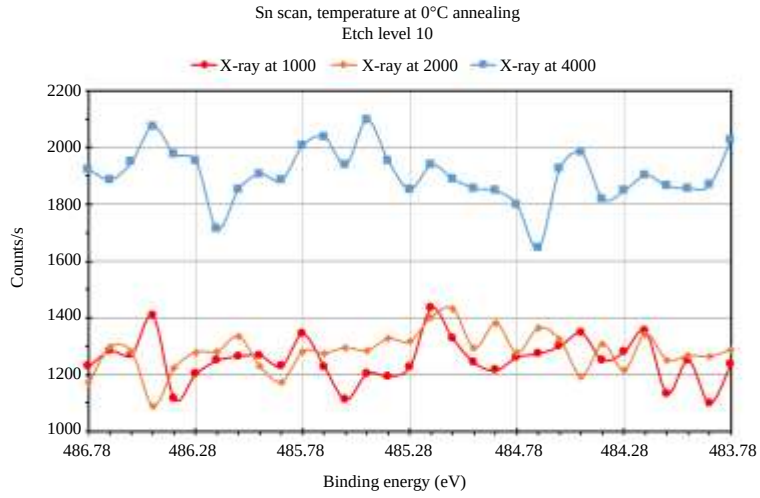

(b)

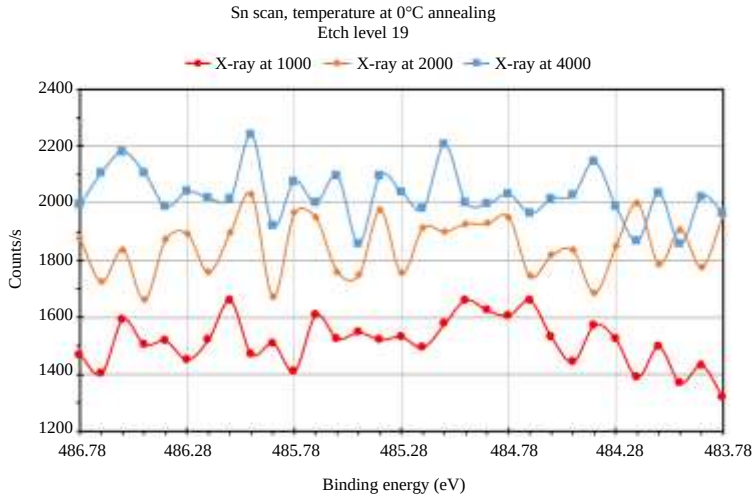

(c)

Fig. 9: (a) Sn Scan at 0 etch level; (b) Sn Scan at 10 etch level (c) Sn Scan at 19 etch level

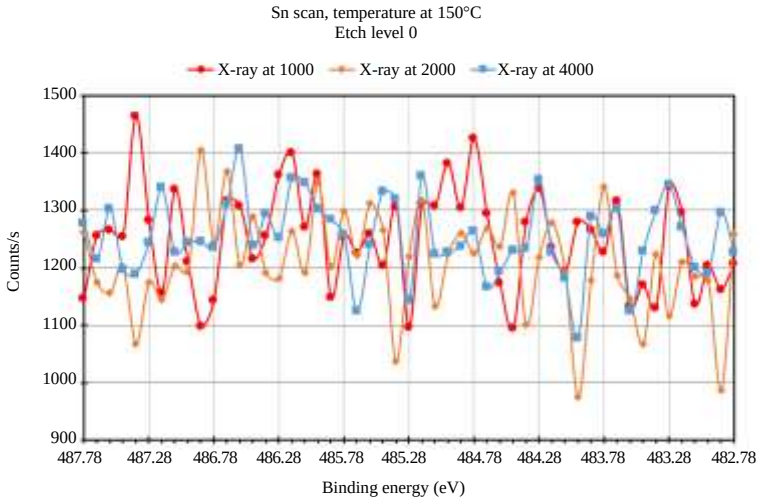

(a)

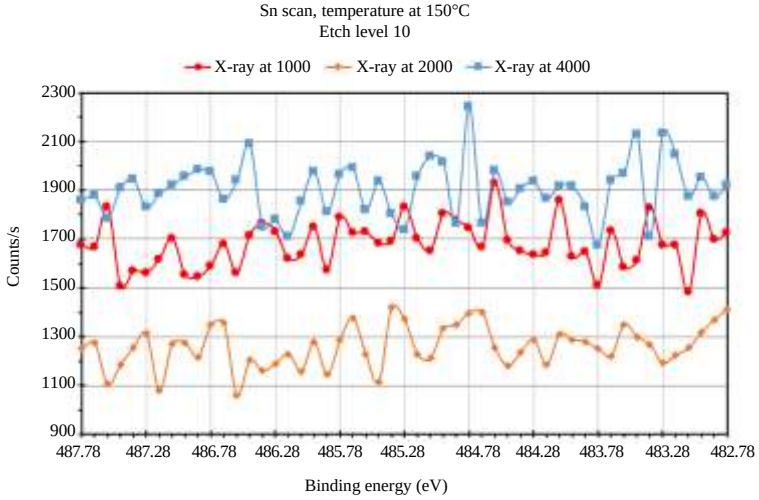

(b)

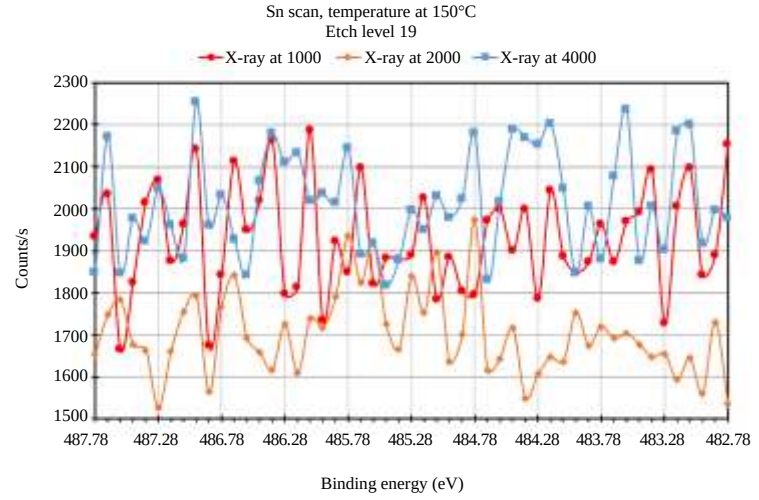

(c)

Fig. 10: (a) Sn Scan at 0 etch level; (b) Sn Scan at 10 etch level; (c) Sn Scan at 19 etch level

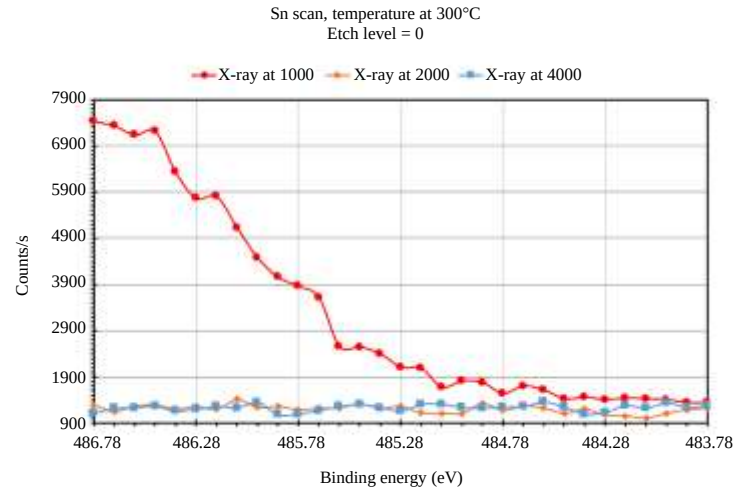

(a)

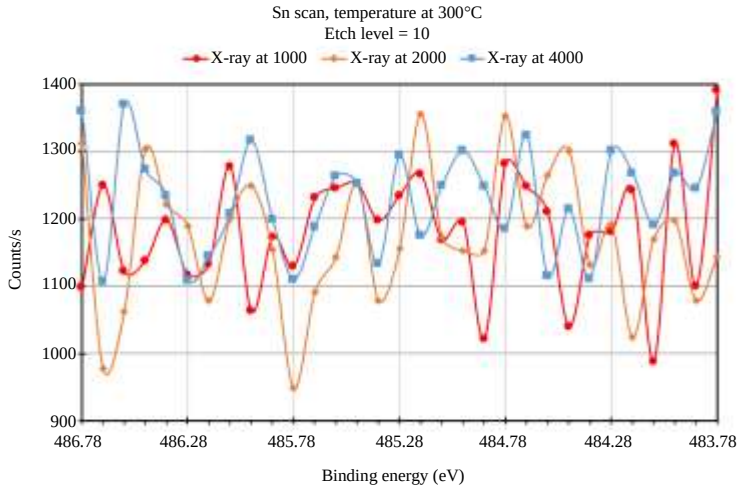

(b)

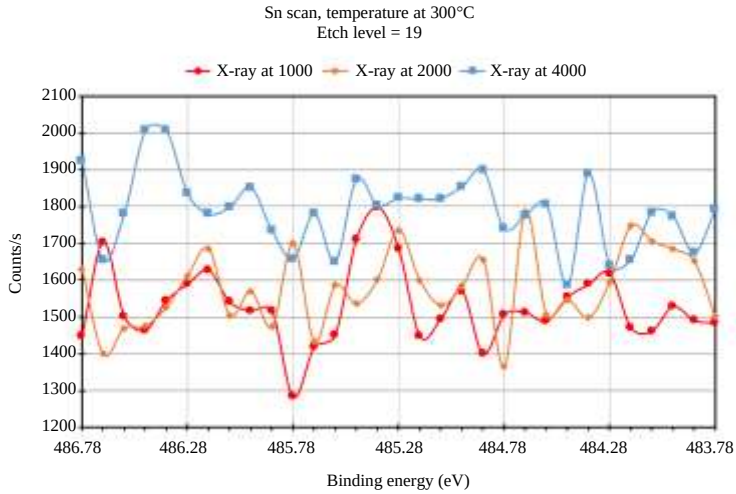

(c)

Fig. 11: (a) Sn Scan at 0 etch level; (b) Sn Scan at 10 etch level; (c) Sn Scan at 19 etch level

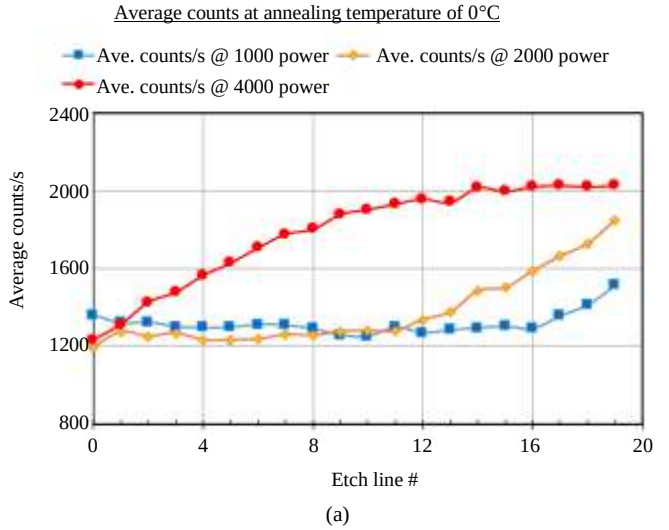

(a)

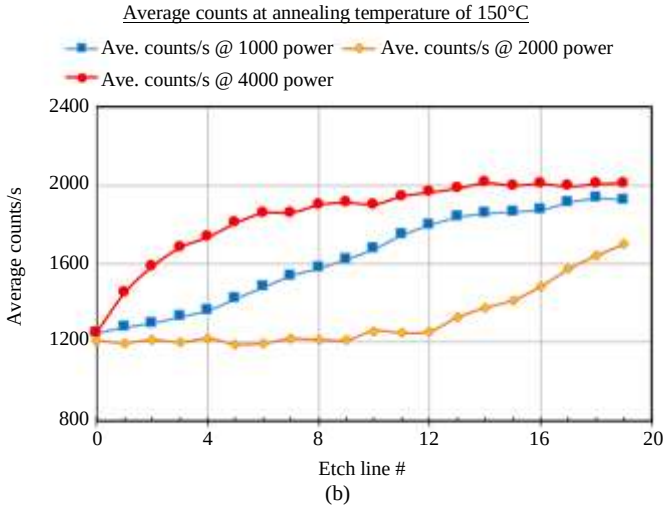

(b)

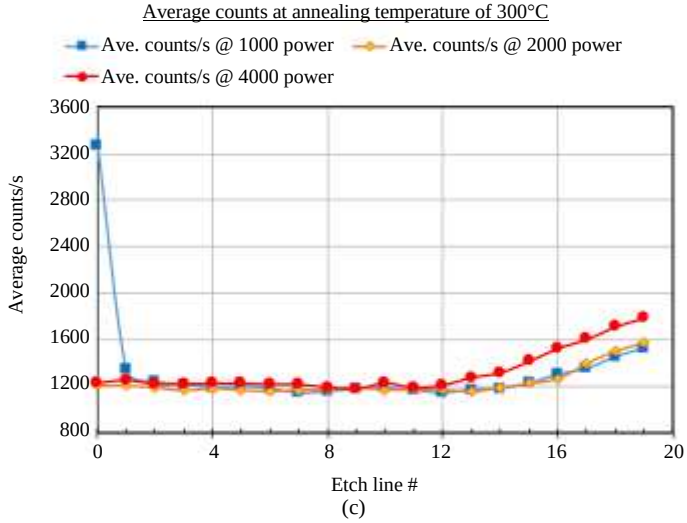

(c)

Fig. 12: (a) Average counts at annealing temperature of 0°C; (b) average counts at annealing temperature of 150°C; (c) average counts at annealing temperature of 300°C

Figure 12b shows the average counts at annealing temperature of 150°C. As seen from Fig. 12b, average count values increase when the x-ray energy increased while the etch line # increased like the case in Fig. 12a for the un-annealed case.

Figure 12c shows the average counts at annealing temperature of 300°C. As seen from Fig. 12c, average count values increase when the x-ray energy increased while the etch line # increased like the case in Fig. 12a and 12b except for three cases of different x-ray energies look overlapped until the etch line # is about 12. The average counts vs etch line # for the annealing of 300°C have lower yields than the cases of un-annealed and annealed at 150°C. This might come from the destruction of the SiO_2 substrates at higher x-ray energy of 4000 eV. For the future studies, the x-ray energy could be chosen less than 4000 eV to reach higher yields.

Figure 13 shows the 3D plot for average counts at different annealing temperatures for un-annealed, annealed at 150°C and annealed at 300°C. In the Fig. 13, T = 0°C corresponds the un-annealed case, T = 150°C corresponds the annealing of SiO_2 substrates at 150°C and T = 300°C corresponds the annealing of SiO_2 substrates at 300°C. Figure 13 is summary and combination of Fig. 12a-12c in 3D case since counts, x-ray energy and energy etch line # was shown at the same time on the same plot. If someone looks from the x-ray energy side, the shift of the number of counts vs etch line 3 could be seen very clearly.

Figure 14a and 14b show Sn3d SnO peak position profile and Sn3d5 peak position profile, respectively for unannealed SiO_2 substrates when the x-ray energies are at 1000, 2000 and 4000 eV. Figure 14-16 show etched depth in nm in the x-axis. Etch depth from 0 to 340 nm were shown in Fig. 14a and 14b. That means that peak positions at different energies of x-ray were gathered when the etching started from the surface to the depth of 340 nm. As seen from Fig. 14a and 14b, peak values could be gathered differently for different energy levels of x-ray since higher energy could diffuse in deeper region due to power of the energy in the SiO_2 substrates.

Figure 15a-15c show Sn3d SnF2 peak position profile, Sn3d SnO peak position profile and Sn3d5 peak position profile, respectively for annealed thin film at 150°C when the x-ray energies are at 1000, 2000 and 4000 eV. Etch depth from 0 to 340 nm were shown in Fig. 15a-15c. As seen from Fig. 14a and 14b, peak values could be gathered differently for different energy levels of x-ray since higher energy could diffuse in deeper region due to power of the energy in the SiO_2 substrates structure for Fig. 15a-15c.

Figure 16a and 16b show Sn3d SnO peak position profile and Sn3d5 peak position profile, respectively for annealed the SiO_2 substrate at 300°C when the x-ray energies are at 1000, 2000 and 4000 eV. Etch depth from 0 to 340 nm were shown in Fig. 16a and 16b. As seen from Fig. 14 and 15, peak values could be gathered differently for different energy levels of x-ray since higher energy could diffuse in deeper region due to power of the energy in the SiO_2 substrate for Fig. 16a and 16b.

Figure 17 shows Sn Scan Temperature at 0 annealing (un-annealed SiO_2 substrate) and X-Ray power = 1000, 2000 and 4000 eV, respectively when the etch level is 0 (surface of the SiO_2 substrate). The sample in Fig. 17 were scanned with respect to Binding energy of values from 483.78 to 486.78 eV. Red straight lines show the places of Sn3d SnO and Sn 3d5 places in the binding energy scale. As seen from Fig. 17, the shapes of counts peak change when the applied x-ray etching energy changed.

Figure 18 shows Sn Scan Temperature at 0 annealing (un-annealed SiO_2 substrate) and X-Ray power = 1000, 2000 and 4000 eV, respectively when the etch level is 10. The sample in Fig. 18 was scanned with respect to Binding energy of values from 483.78 to 486.78 eV. Red straight lines show the places of Sn3d SnO and Sn 3d5 places in the binding energy scale. As seen from Fig. 18, the shapes of counts peak change when the applied x-ray etching energy changed.

Figure 19 show Sn Scan Temperature at 0 annealing (un-annealed SiO_2 substrate) and X-Ray power = 1000, 2000 and 4000 eV, respectively when the etch level is 19. The sample in Fig. 19 was scanned with respect to Binding energy of values from 483.78 to 486.78 eV. Red straight lines show the places of Sn3d SnO and Sn 3d5 places in the binding energy scale. As seen from Fig. 19, the shapes of counts peak change when the applied x-ray etching energy changed.

Figure 20 shows Sn Scan, Temperature at 150°C annealing and X-Ray power = 1000, 2000 and 4000 eV, respectively when the etch level is 0. The sample in Fig. 20 was scanned with respect to Binding energy of values from 482.78 to 487.78 eV. Red straight lines show the places of Sn3d SnF2, Sn3d SnO and Sn 3d5 places in the binding energy scale. As seen from Fig. 20, the shapes of counts peak change when the applied x-ray etching energy changed.

Figure 21 show Sn Scan, Temperature at 150°C annealing and X-Ray power = 1000, 2000 and 4000 eV, respectively when the etch level is 10. The sample in Fig. 21 was scanned with respect to Binding energy of values from 482.78 to 487.78 eV. Red straight lines show the places of Sn3d SnF2, Sn3d SnO and Sn 3d5 places in the binding energy scale. As seen from Fig. 21, the shapes of counts peak change when the applied x-ray etching energy changed.

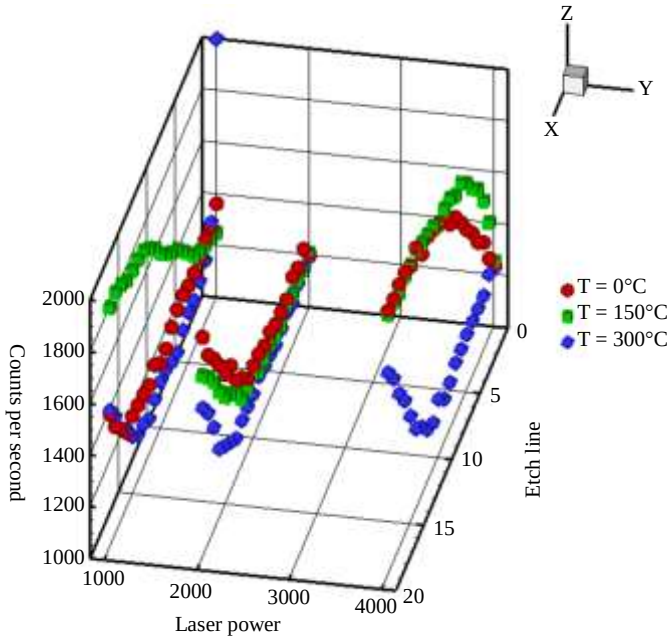

Fig. 13: 3D plot for average counts at different annealing temperature

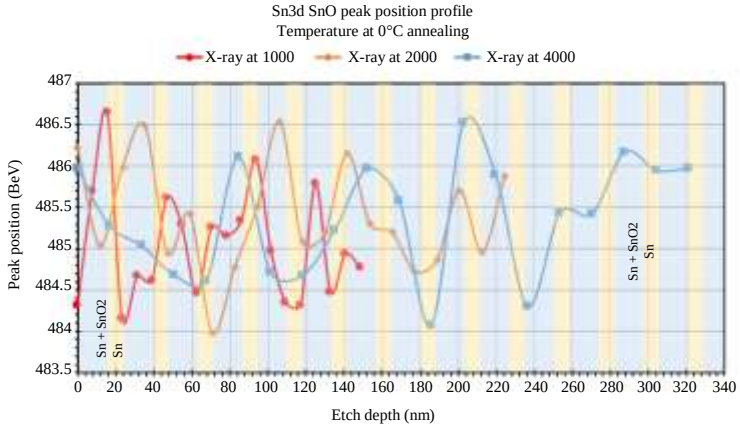

(a)

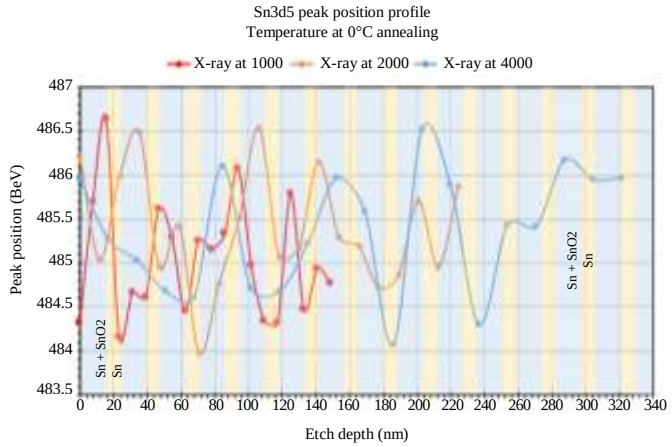

(b)

Fig. 14: (a) Sn3d SnO peak position profile at 0°C annealing; (b) Sn3d5 peak position profile at 0°C annealing

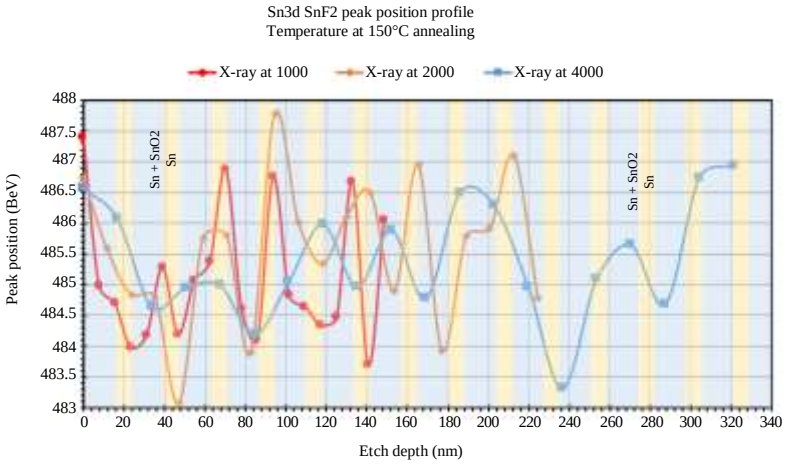

(a)

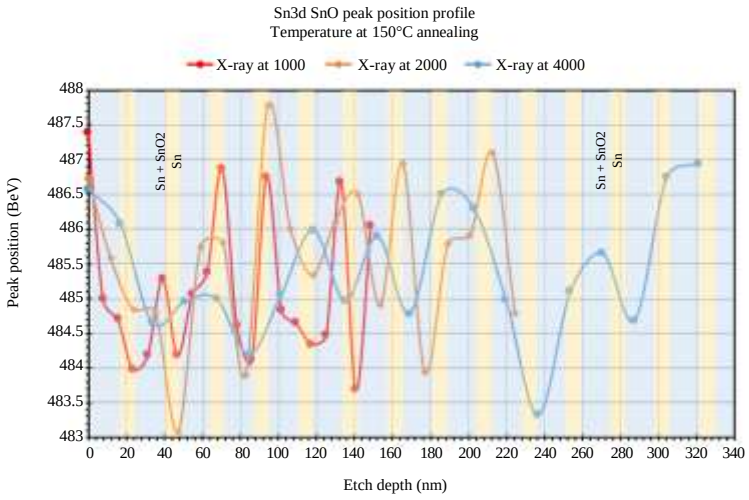

(b)

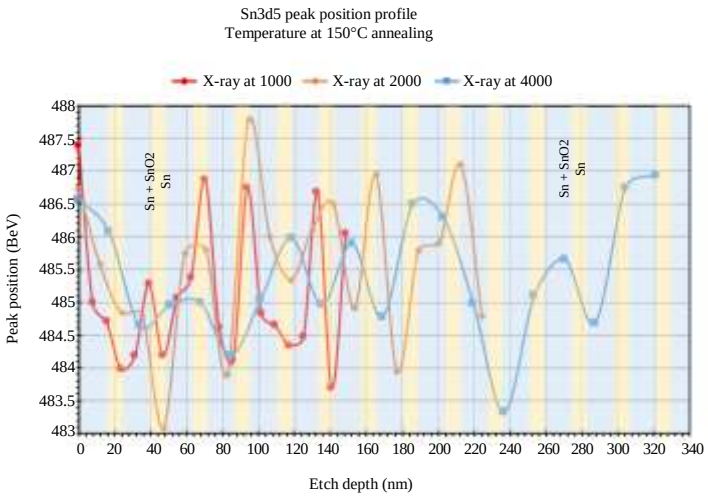

(c)

Fig. 15: (a) Sn3d SnF2 peak position profile at 150°C annealing; (b): Sn3d SnO peak position profile at 150°C annealing (c) Sn3d5 peak position profile at 150°C annealing

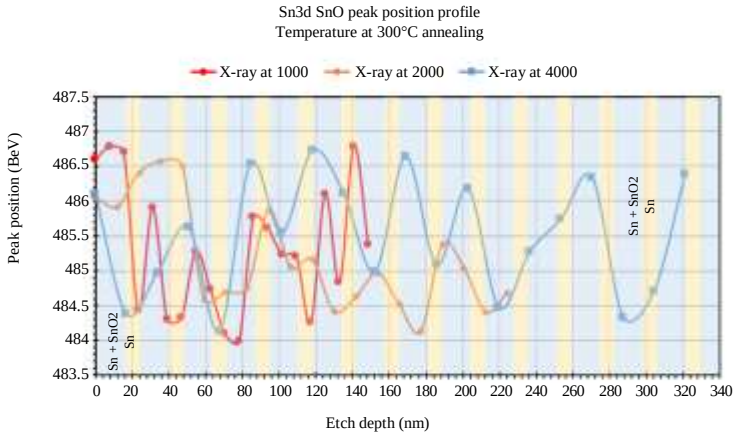

(a)

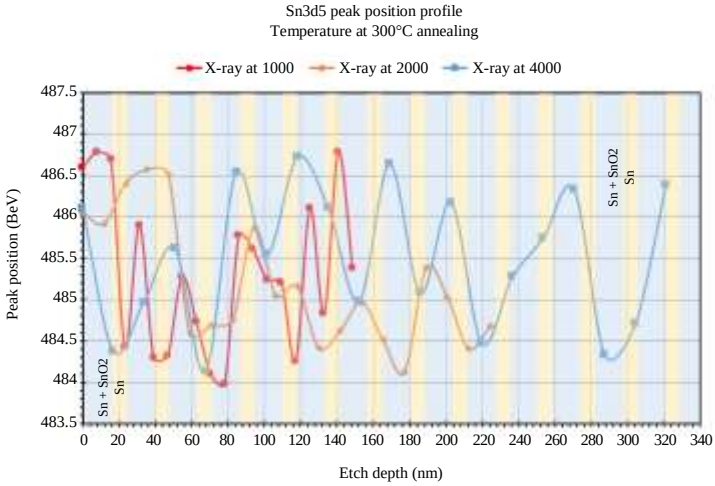

(b)

Fig. 16: (a) Sn3d SnO peak position profile at 300°C annealing; (b) Sn3d5 peak position profile at 300°C annealing

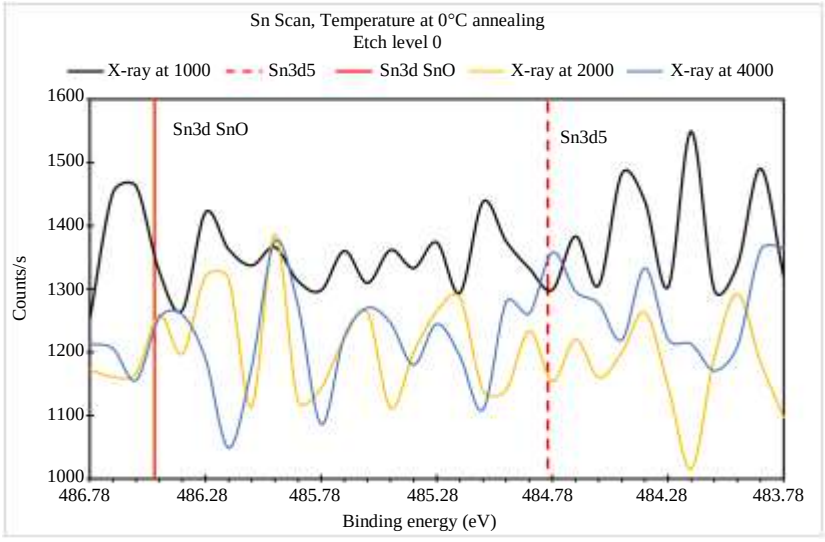

Fig. 17: Sn Scan, Temperature at 0 annealing (un-annealing) and X-Ray = 1000, X-Ray = 2000 and X-Ray = 4000 on the SiO_2 substrates

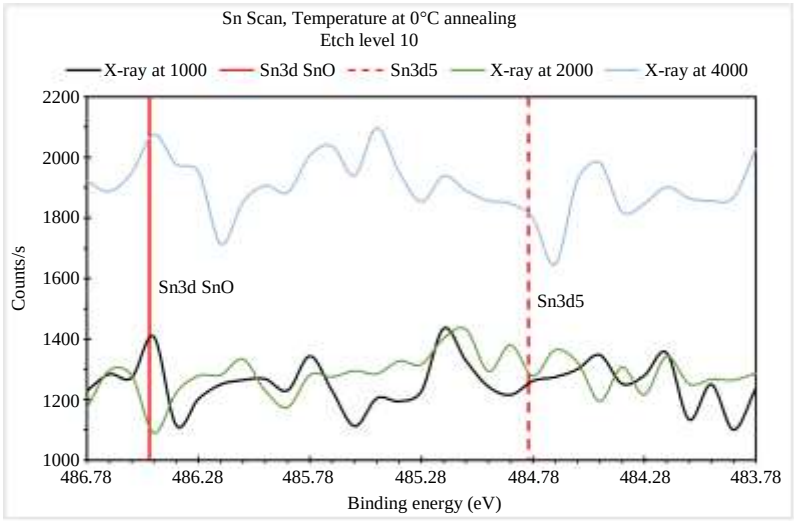

Fig. 18: Sn Scan, Temperature at 0 annealing (un-annealing) and X-Ray = 1000, X-Ray = 2000 and X-Ray = 4000 on the SiO_2 substrates

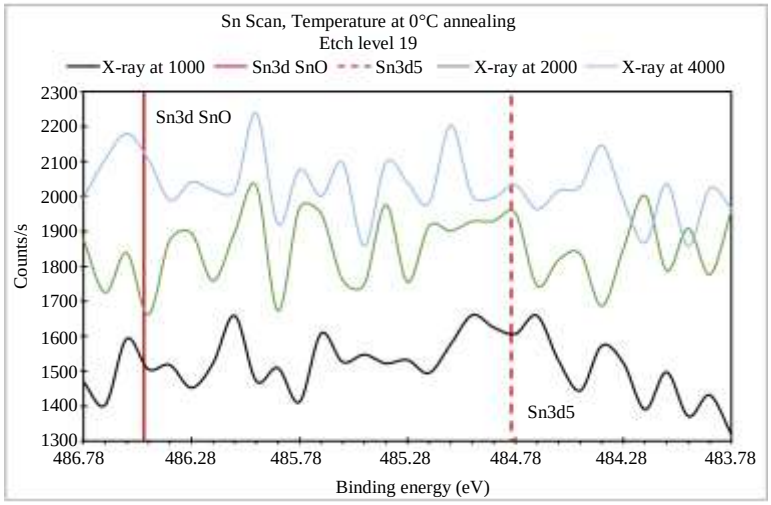

Fig. 19: Sn Scan, Temperature at 0 annealing (un-annealing) and X-Ray = 1000, X-Ray = 2000 and X-Ray = 4000 on the SiO_2 substrates

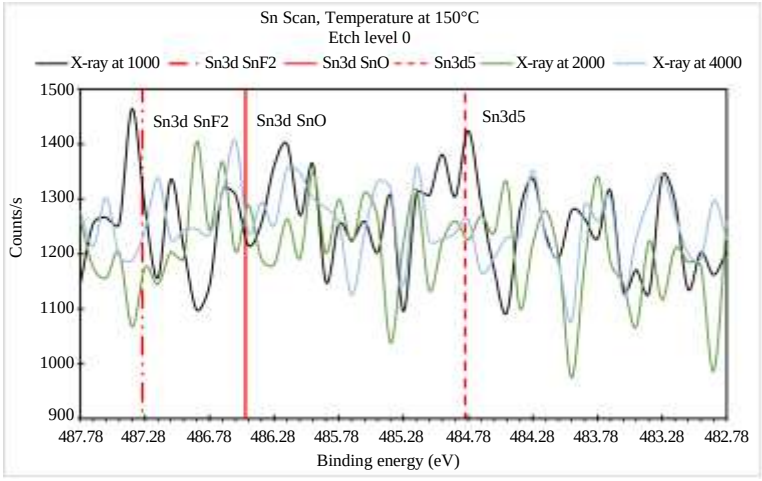

Fig. 20: Sn Scan, Temperature at 150°C annealing and X-Ray = 1000, X-Ray = 2000 and X-Ray = 4000 on the SiO_2 substrates

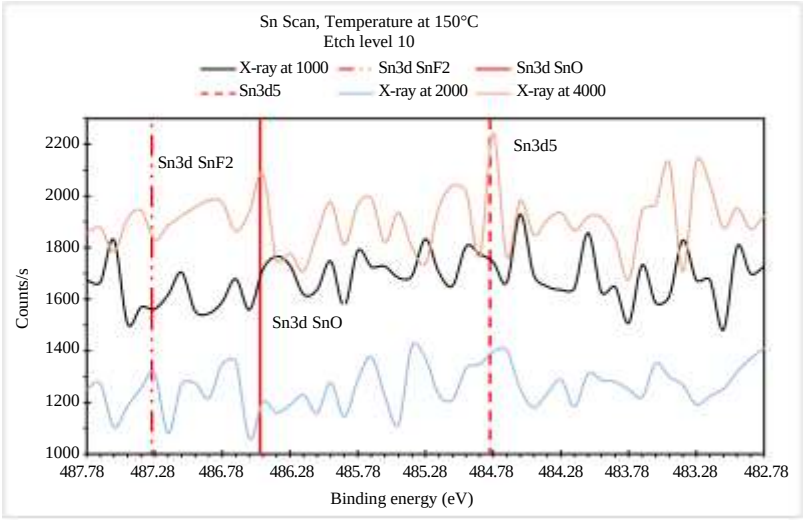

Fig. 21: Sn Scan, Temperature at 150°C annealing and X-Ray = 1000, X-Ray = 2000 and X-Ray = 4000 on the SiO_2 substrates

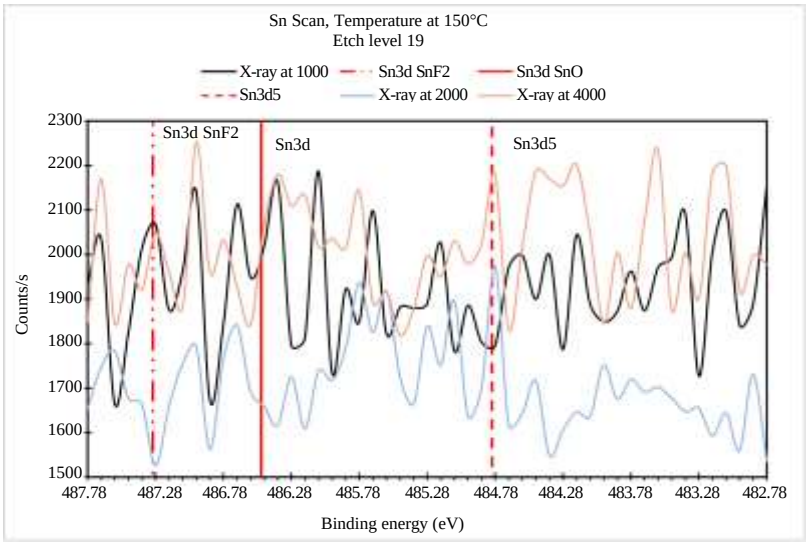

Fig. 22: Sn Scan, Temperature at 150°C annealing and X-Ray = 1000, X-Ray = 2000 and X-Ray = 4000 on the SiO_2 substrates

Figure 22 show Sn Scan, Temperature at 150°C annealing and X-Ray power = 1000, 2000 and 4000 eV, respectively when the etch level is 19. The sample in Fig. 22 was scanned with respect to Binding energy of values from 482.78 to 487.78 eV. Red straight lines show the places of Sn3d SnF2, Sn3d SnO and Sn 3d5 places in the binding energy scale. As seen from Fig. 22, the shapes of counts peak change when the applied x-ray etching energy changed.

Figure 23 show Sn Scan Temperature at 300°C annealing and X-Ray power = 1000, 2000 and 4000 eV, respectively when the etch level is 0 (surface of the SiO_2 substrate). The sample in Fig. 23 was scanned with respect to Binding energy of values from 483.78 to 486.78 eV like unannealed case. Red straight lines show the places of Sn3d SnO and Sn 3d5 places in the binding energy scale like unannealed case. The Sn3d SnF2 peak disappeared. As seen from Fig. 23, the shapes of counts peak change when the applied x-ray etching energy changed.

Figure 24 show Sn Scan, Temperature at 300°C annealing and X-Ray power = 1000, 2000 and 4000 eV, respectively when the etch level is 10. The sample in Fig. 24 was scanned with respect to Binding energy of values from 483.78 to 486.78 eV like un-annealed case. Red straight lines show the places of Sn3d SnO and Sn 3d5 places in the binding energy scale like un-annealed case. The Sn3d SnF2 peak also disappeared here. As seen from Fig. 24, the shapes of counts peak change when the applied x-ray etching energy changed.

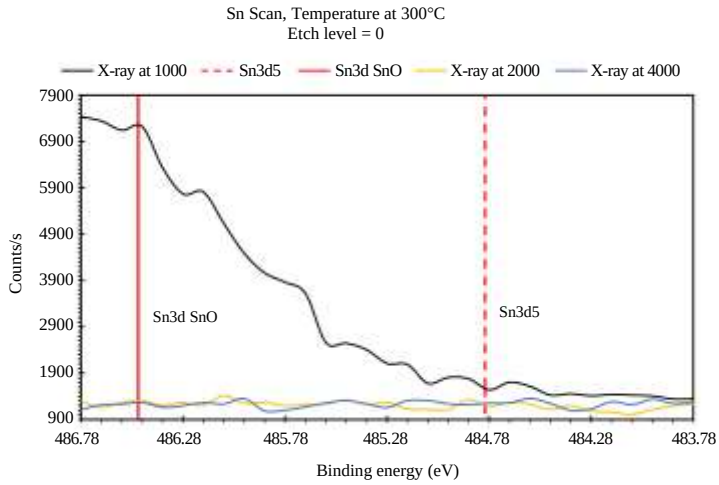

Fig. 23: Sn Scan, Temperature at 300°C annealing and X-Ray = 1000, X-Ray = 2000 and X-Ray = 4000 on the SiO_2 substrates

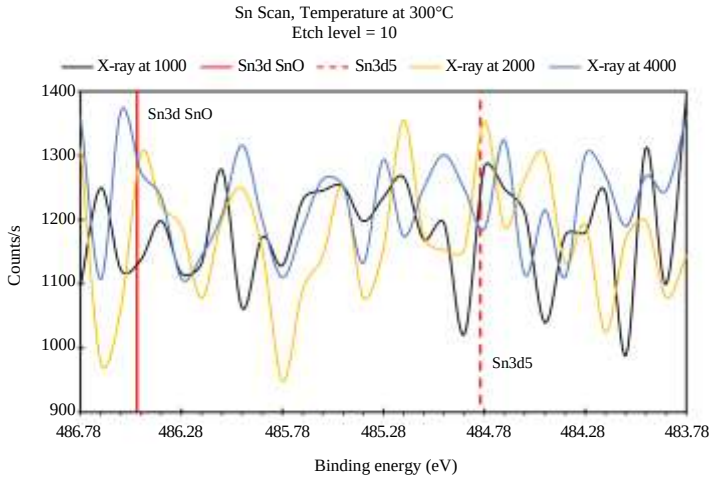

Fig. 24: Sn Scan, Temperature at 300°C annealing and X-Ray = 1000, X-Ray = 2000 and X-Ray = 4000 on the SiO_2 substrates

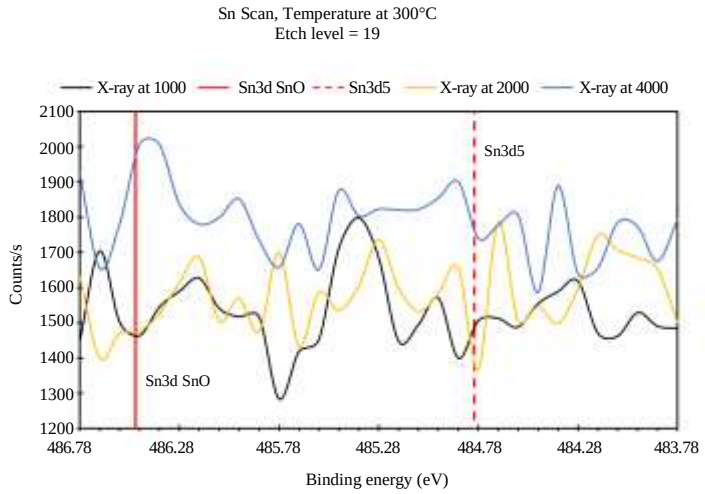

Fig. 25: Sn Scan, Temperature at 300°C annealing and X-Ray = 1000, X-Ray = 2000 and X-Ray = 4000 on the SiO_2 substrates

Figure 25 show Sn Scan, Temperature at 300°C annealing and X-Ray power = 1000, 2000 and 4000 eV, respectively when the etch level is 19. The sample in Fig. 25 was scanned with respect to Binding energy of values from 483.78 to 486.78 eV like un-annealed case. Red straight lines show the places of Sn3d SnO and Sn 3d5 places in the binding energy scale like un-annealed case. The Sn3d SnF2 peak was also not seen here. As seen from Fig. 25, the shapes of counts peak change when the applied x-ray etching energy changed. It seems that Sn3d SnF2 peak just appeared when the SiO_2 substrate was annealed at 150°C.

Figure 26-28 show Full Width at Half Maximum (FWHM) for SnO at 0°C (unannealed), annealed at 150°C and annealed at 300°C, respectively. FWHM vs Etch Depth in nm were plotted for different x-ray energies of 1000, 2000 and 4000 eV. As seen from the Figure, etching levels starts from the surface up to 320 nm using different x-ray energies. Figure 22-24 show that if the x-ray energy power increased from 1000 to 4000 eV, the depth profile changed and reached deeper etching level. By this way, more information could be gathered from deeper levels of the SiO_2 substrate. The changes in FWHM values could come from the power of x-rays and the depth profile of the etched materials. This gives very useful information about the materials. The Full Width at Half Maximum (FWHM) are useful indicators of chemical state changes and physical influences. That is, broadening of a peak may indicate: A change in the number of chemical bonds contributing to a peak shape, a change in the sample condition (x-ray damage) and/or differential charging of the surface (localized differences in the charge state of the surface) (Casa XPS, 2020).

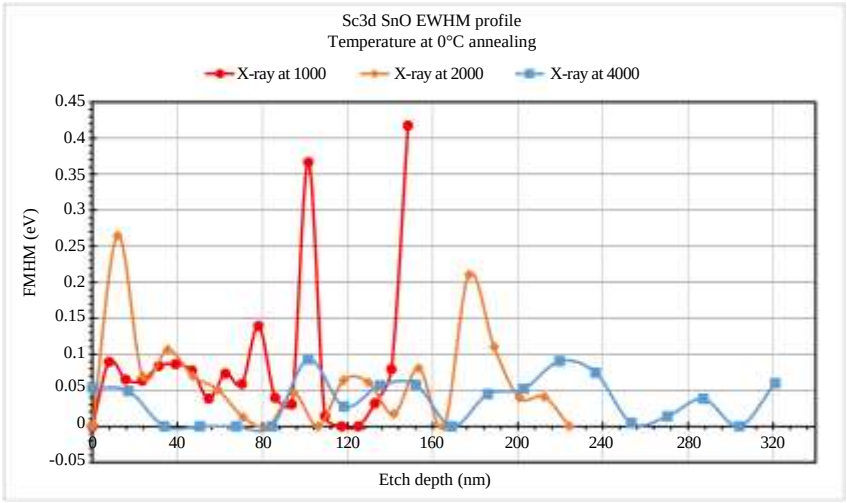

Fig. 26: FWHM for SnO at 0°C on the SiO_2 substrates

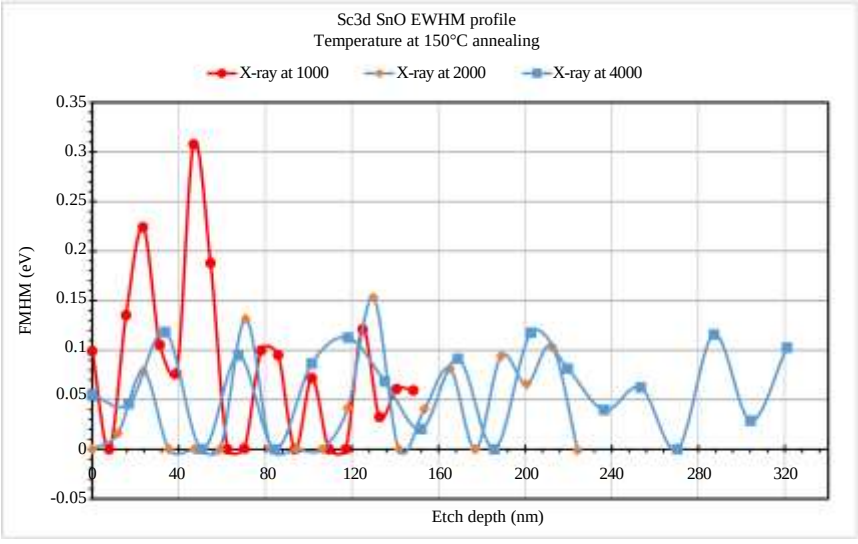

Fig. 27: FWHM for SnO at 150°C on the SiO_2 substrates

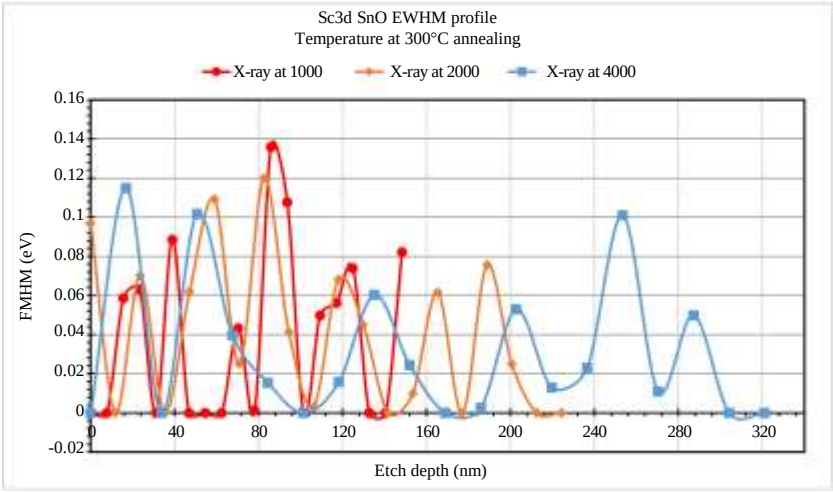

Fig. 28: FWHM for SnO at 300°C on the SiO_2 substrates

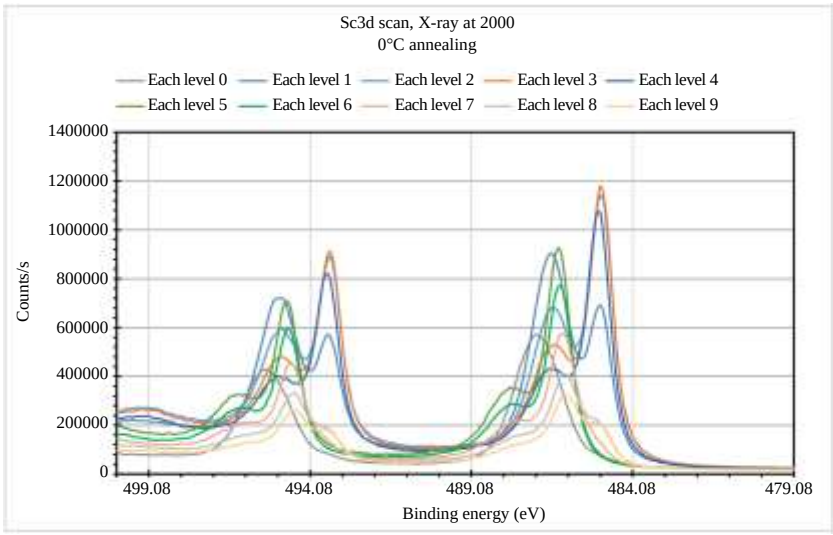

Fig. 29: Sn3d Scan, Temperature at 0°C annealing (un-annealing) and X-Ray = 2000 for 10 etch levels for the thin films of Sn/Sn+SnO_2

XPS Studies on the Thin Films of Sn/Sn+SnO_2 on the SiO_2 Substrates

After the detailed XPS studies on the SiO2 substrates as shown in Fig. 9 to 28, we would like to show XPS analysis for the multilayered Sn/Sn+SnO_2 thin films. The geometry was shown before in Fig. 8 for the multilayered thin film structure. The XPS studies on the multilayered Sn/Sn+SnO_2 thin films were shown in the Fig. 29 to 37.

Figure 29 shows the Sn3d Scan, when the temperature at 0°C annealing (un-annealing) and X-Ray = 2000 for 10 etch levels for the thin films of Sn/Sn+SnO_2. As seen from Fig. 29, there are chemical shifts towards lower binding energy. There are 10 etch levels on Fig. 29. Chemical shifts give information about the chemical structure and oxidation level of the thin film. There are shifting among the peaks even if the etch level goes to deeper levels. It is imperative to consider the reason for the apparent BE differences between photoelectrons originating from the same core-level in atoms with different chemical environment (Greczynski and Hultman, 2020). Lv *et al*. (2010) studied XPS study on Sb_2Te_3 thin films. They have gathered XPS spectra from unannealed and annealed Sb_2Te_3 thin films. They did not perform etch depth profile but their peaks look similar to our work with different binding energies. Their higher peak showed up at about 570 eV and lower peak showed at about 582 eV for unannealed thin film while the highest peak showed up around 572 eV and the lowest peak showed up around 582 eV for annealed at 613 K from Te 3d spectra. Similar spectra could be seen from Sb 3d scan from their samples. Their Sb 3d

peak has the highest peak value at about 540 eV and the lowest peak at about 530 eV. Chemical shifts through the binding energies could come from the type of scan and the difference of elemental structure. The current study has similar spectra like the Sb_2Te_3 spectra performed by Lv *et al*. Our cases have lower binding energies than the Sb_2Te_3 performed by Lv *et al*., The reason might come from our film structures since we have Sn and SnO_2 multilayer structures.

Barreca *et al*. (2000) studied XPS studies on SnO_2 nanocrystalline structure. Their highest peak showed around 490 eV while the lowest peak showed up around 487 eV. Our structure has some similarity from the binding energy values. Our difference could come from Sn and SnO2 multilayers while Barreca *et al*. studied the nanocrystalline structure of thin film. In Fig. 30, etching levels of 0, 5 and 9 were plotted to show the peak differences in detail.

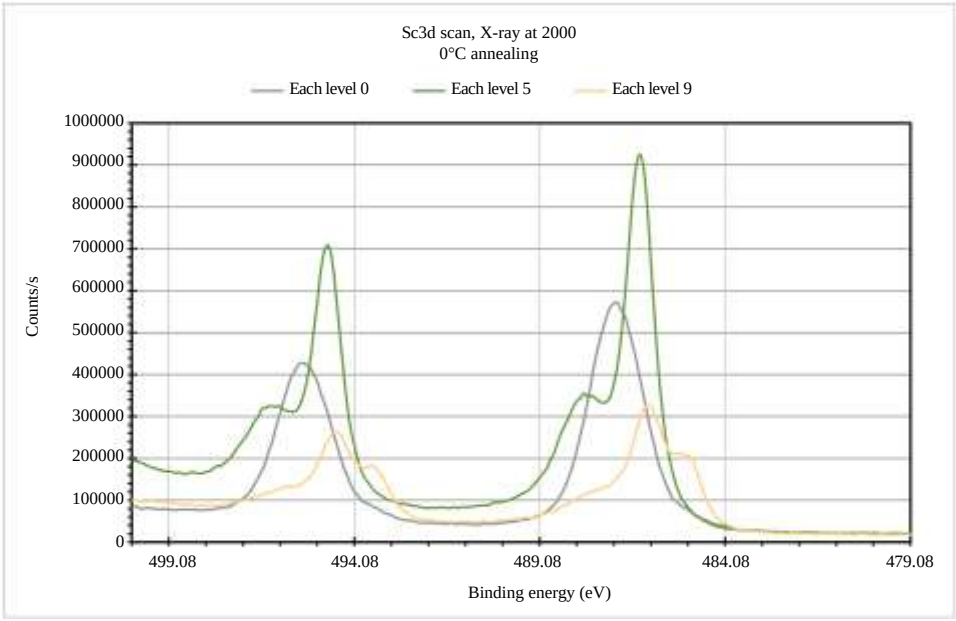

Fig. 30: Sn3d Scan, Temperature at 0°C annealing (un-annealing) and X-Ray = 2000 for 0, 5 and 9 etch levels for the thin films of Sn/Sn+SnO_2

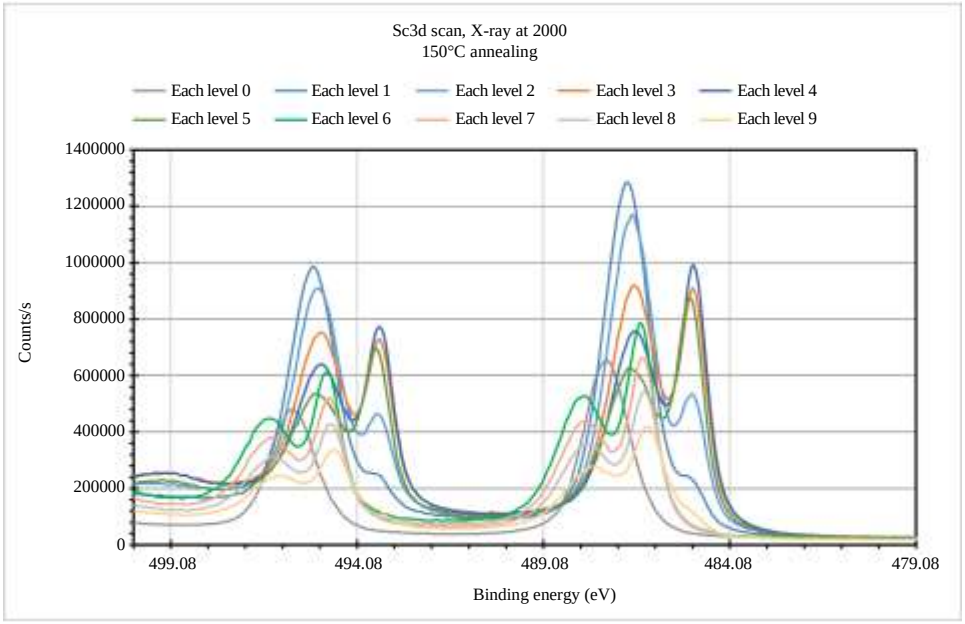

Fig. 31: Sn3d Scan, Temperature at 150°C annealing and X-Ray = 2000 for 10 etch levels for the thin films of Sn/Sn+SnO_2

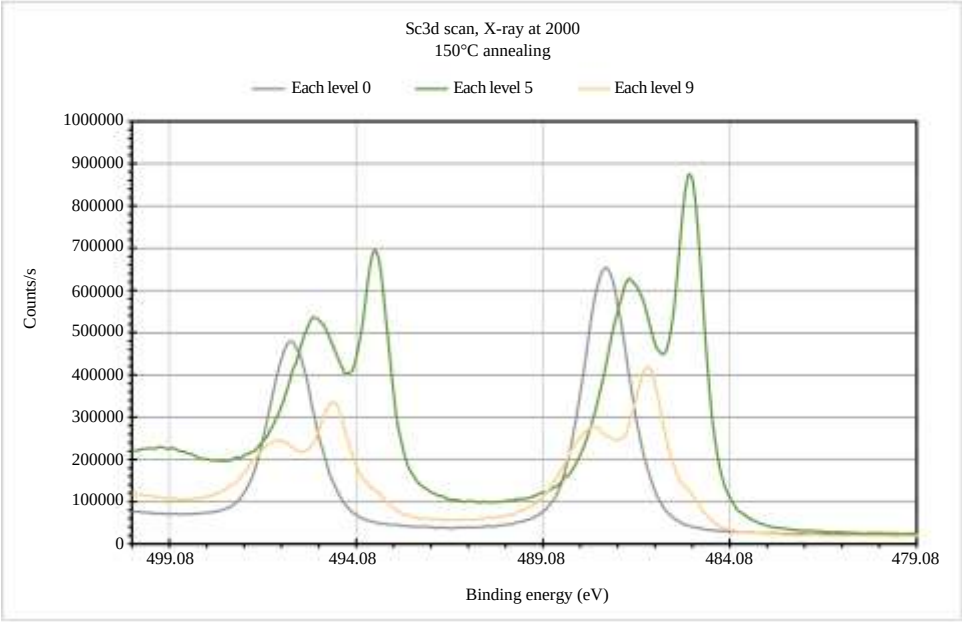

Fig. 32: Sn3d Scan, Temperature at 150ºC annealing and X-Ray = 2000 for 0, 5 and 9 etch levels for the thin films of Sn/Sn+SnO_2

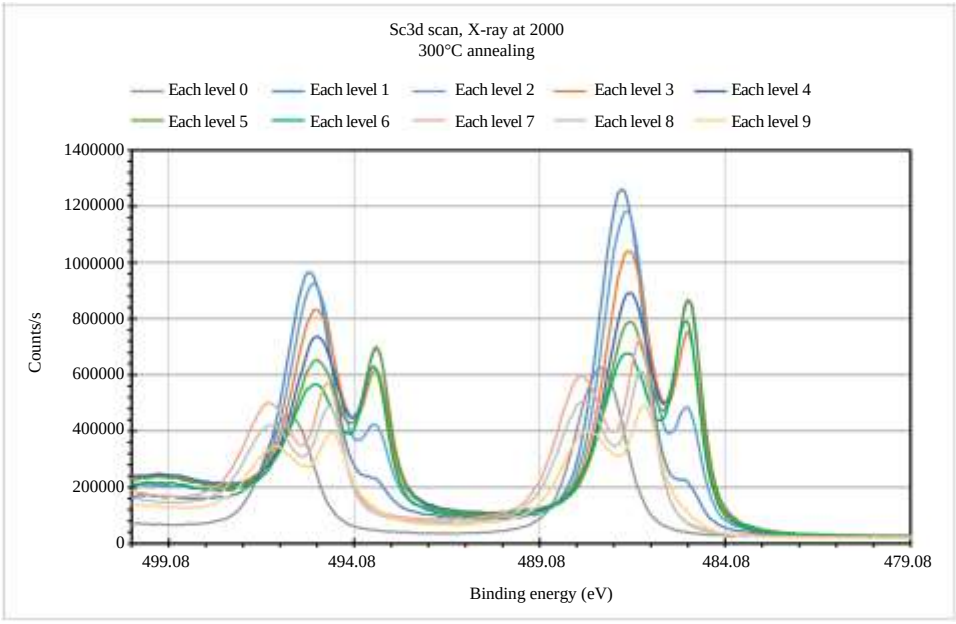

Fig. 33: Sn3d Scan, Temperature at 300°C annealing and X-Ray = 2000 for 10 etch levels for the thin films of Sn/Sn+SnO_2

Figure 31 shows the similar scan like discussed in Fig. 29. Only difference is the thin film system was annealed at 150°C. Even the spectra in Fig. 29 and 31 look like each other, there are some differences on the intensities of the peak and shifting around themselves. Figure 32 shows the selected etched values of 0, 5 and 9 for the annealed thin films at 150°C. The differences between the annealing effects between unannealed and annealed at 150°C could be seen more clearly at Fig. 30 and 32.

Figure 33 shows the annealing effects on the thin film at 300°C. Even Fig. 33 looks like Fig. 29 and 31. To see the details of the differences among the peak values and shifting in binding energies, the Fig. 30, 32 and 34 should be studied.

The chemical shift and differences among the peaks and their binding energies could be seen clearly at Fig. 35-37 since those peaks were plotted for different etching level. Figure 35 shows the binding energy curves when the etch

level is 0 (surface of the thin films). Unannealed and annealed at 150 and 300°C peaks were plotted. The changes among the curves could be seen clearly addition to the shift in peaks. Figure 36 shows the similar relation when the etch number or etch level is 5. The peak levels and shifts in the peaks with respect to the binding energies could be seen clearly. Figure 37 shows the similar behavior when the etch number 9 for three different cases of films including unannealed and annealed at 150 and 300°C. The peaks at the etches level of 5 and 9 are look like to each other but different than the surface case of etch number 1. When the etching number goes high in other words going to the deeper level of thin films, the peaks started to have some splitting on the peaks. This might give some information about the binding energies among the chemical structures. In our future works, we are planning to work and understand in mire details of these splitting on the peaks. Like performed some experiments on the SiO_2 substrates, we would like to perform similar studies on the thin film cases like FWHM.

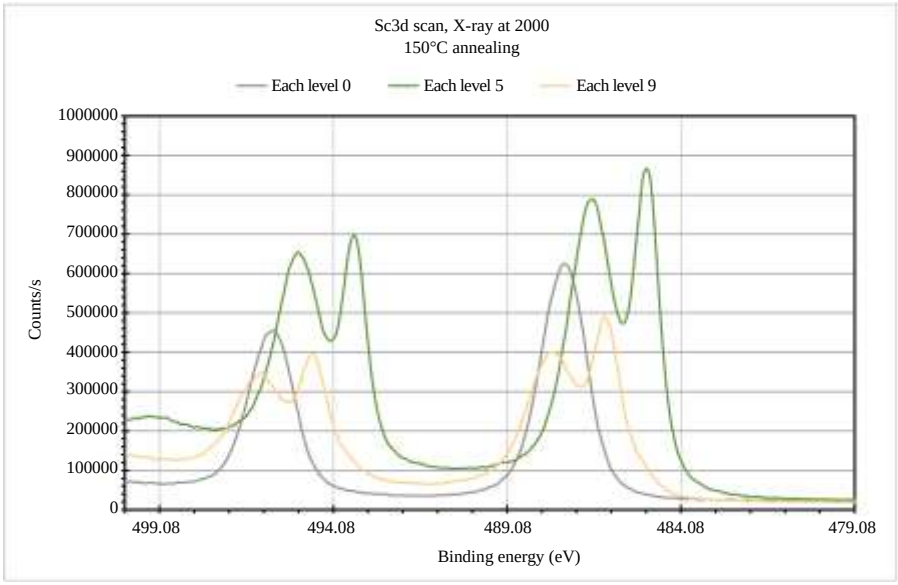

Fig. 34: Sn3d Scan, Temperature at 300°C annealing and X-Ray = 2000 for 0, 5 and 9 etch levels for the thin films of Sn/Sn+SnO_2

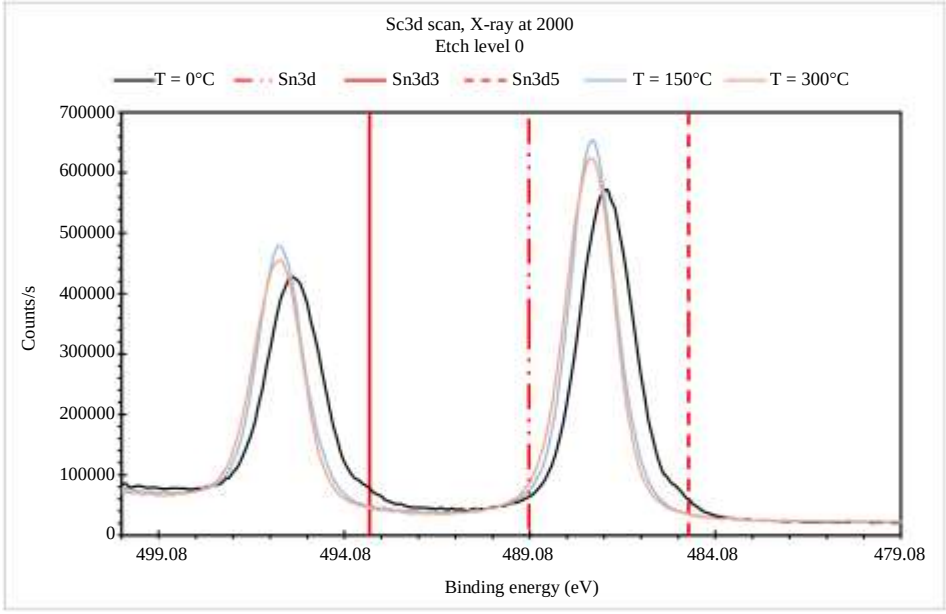

Fig. 35: Sn3d Scan, X-Ray = 2000 at 0 etch level for annealing temperatures of 0°C (un-annealing), 150 and 300°C for the thin films of Sn/Sn+SnO_2

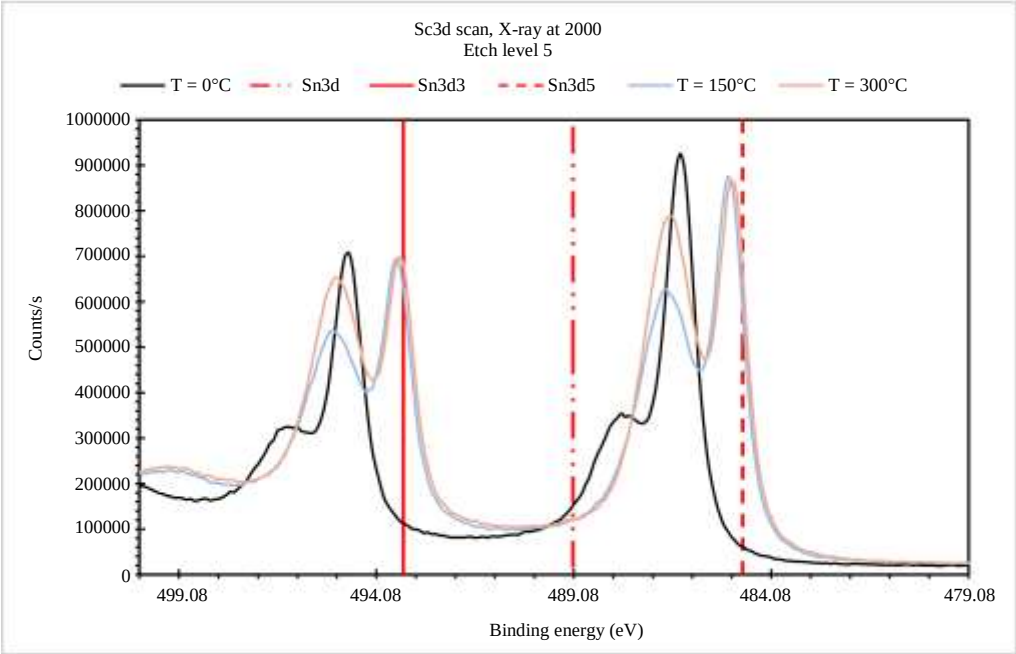

Fig. 36: Sn3d Scan, X-Ray = 2000 at 5 etch level for annealing temperatures of 0°C (un-annealing), 150 and 300°C for the thin films f $Sn/Sn+SnO_2$

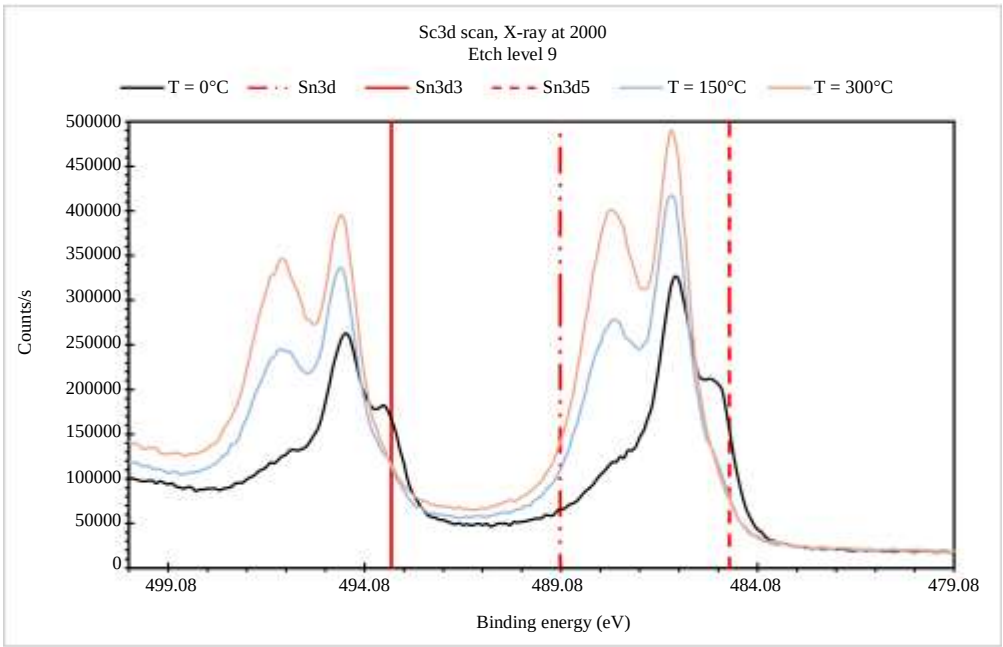

Fig. 37: Sn3d Scan, X-Ray = 2000 at 9 etch level for annealing temperatures of 0°C (un-annealing), 150 and 300°C for the thin films of $Sn/Sn+SnO_2$

Conclusion

Multilayered of thermoelectric $Sn/Sn+SnO_2$ thin films were prepared using KJL DC/RF magnetron sputtering system under Ar gas plasma on the SiO_2 substrates. The thicknesses of the fabricated thin films were found using Filmetrics UV thickness measurement system. The fabricated thin films were annealed at different temperatures to tailor the thermoelectric properties. In this study, unannealed, annealed at 150 and 300°C samples and SiO_2 substrates were characterized using Thermo-Fisher XPS system brought to the Alabama A&M

University by the NSF-MRI support. Thermal treatment of the multilayered thin films has caused some changes of the XPS characterization including binding energy, depth profile, peak value and FWHM. When the x-ray energy power for etching the surfaces through the deeper level of the multilayer thin films, some different information gathered for the average count, binding energy, peak values and FWHM. As the energy increased, some of the FWHM peaks show some broadening even though they are not at a high level with respect to the peaks at lower energy levels. This could give some information about the possible destruction and possible new bonds occurring among the materials. In our future research, we will focus on similar material systems first to characterize the XPS properties of these types of thermoelectric materials since those materials have promising results for energy conversion from waste of heat to electricity. Some of our works performed on the thermoelectric properties of the multilayered thin films structures can be seen in references (Drabo and Budak, 2019; Budak *et al*., 2017; 2016).

Acknowledgement

The authors would like to thank Mr. Bennie Mwaanga Mwiinga for his support and technical assistance throughout this project. The authors would also like to thank the Department of Energy (DOE), National Nuclear Security Administration (NNSA) and the National Science Foundation (NSF) for their financial support.

Funding Information

This project was supported by Department of Energy (DOE) & Nuclear Security Administration (NNSA) with Contract# DE-NA0001896 and DE-NA0002687. The National Science Foundation Historically Black Colleges and Universities Research Infrastructure for Science and Engineering (NSF-HBCU-RISE) with the proposal number of 1546965; and National Science Foundation Major Research Instrumentation (NSF-MRI) program with the award number of 1828729.

Author's Contributions

Each author of this manuscript made considerable contributions in conducting the experimental testing, data-analysis and contributed to the writing of this manuscript.

Ethics

References

Barreca, D., Garon, S., Tondello, E., & Zanella, P. (2000). SnO2 nanocrystalline thin films by XPS. Surface Science Spectra, 7(2), 81-85.

Budak, S., Xiao, Z., Cole, J., Price, D., Davis, T., Strong, T., & Alim, M. A. (2017). Thermoelectric and optical properties of advanced thermoelectric devices from Ni/Bi2Te3/Ni and Ni/Sb2Te3/Ni thin films. Journal of Vacuum Science & Technology B, Nanotechnology and Microelectronics: Materials, Processing, Measurement and Phenomena, 35(5), 051401.

Budak, S., Xiao, Z., Johnson, B., Cole, J., Drabo, M., Tramble, A., & Casselberry, C. (2016). Highly-Efficient Advanced Thermoelectric Devices from Different Multilayer Thin Films. American Journal of Engineering and Applied Sciences. 9(2), 356–363.

Casa XPS. (2020). Basic Quantification of XPS Spectra. Casa XPS. http://www.casaxps.com

Drabo, M., & Budak, S. (2019). Thermoelectric and optical properties of advanced thermoelectric devices from different multilayer thin films. American Journal of Applied Sciences. 16(8), 225.237.

Geng, S., Zhang, S., & Onishi, H. (2002). XPS applications in thin films research. Materials Technology, 17(4), 234-240.

Gould, R. D., Kasap, S., & Ray, A. K. (2017). Thin films. In Springer Handbook of Electronic and Photonic Materials (pp. 1-1). Springer, Cham.

Greczynski, G., & Hultman, L. (2020). X-ray photoelectron spectroscopy: Towards reliable binding energy referencing. Progress in Materials Science, 107, 100591.

Koçak, A. (2018). Thin film preparation, particle size and thickness analysis experimental report. Tusas Engine Industries, Inc.

Lv, B., Hu, S., Li, W., Di, X., Feng, L., Zhang, J., ... & Lei, Z. (2010). Preparation and Characterization of Thin Films by Coevaporation. International Journal of Photoenergy, 2010.

Mao, S. F., Zhang, Z. M., Tokesi, K., Csik, A., Toth, J., Bereczky, R. J., & Ding, Z. J. (2008). XPS analysis of nano-thin films on substrate. Surface and Interface Analysis: An International Journal devoted to the development and application of techniques for the analysis of surfaces, interfaces and thin films, 40(3-4), 728-730.

NACK Network, Pennsylvania State University. (2018). X-Ray Photoelectron Spectroscopy (XPS) [Slides]. Pennsylvania State University.

Seah, M. P., Spencer, S. J., Bensebaa, F., Vickridge, I., Danzebrink, H., Krumrey, M., & Azuma, Y. (2004). Critical review of the current status of thickness measurements for ultrathin SiO2 on Si Part V: Results of a CCQM pilot study. Surface and Interface Analysis: An International Journal devoted to the development and application of techniques for the analysis of surfaces, interfaces and thin films, 36(9), 1269-1303.

Teixeira, V., Carneiro, J., Carvalho, P., Silva, E., Azevedo, S., & Batista, C. (2011). High barrier plastics using nanoscale inorganic films. In Multifunctional and nano-reinforced polymers for food packaging (pp. 285-315). Woodhead Publishing.

Thermo Scientific XPS. (2020). What is XPS. https://xpssimplified.com/whatisxps.php

Washington State University, & Scudiero, L. (2019). X-Ray Photoelectron Spectroscopy (XPS) [Slides]. Washington State University.

Xie, L., Abliz, D., & Li, D. (2014). Thin Film Coating for Polymeric Micro Parts.

Zhong, J. Q., Wang, M., Hoffmann, W. H., van Spronsen, M. A., Lu, D., & Boscoboinik, J. A. (2018). Synchrotron-based ambient pressure X-ray photoelectron spectroscopy of hydrogen and helium. Applied Physics Letters, 112(9), 091602.